Nanoscale

COMMUNICATION

View Article Online
View Journal | View Issue

Cite this: *Nanoscale*, 2015, **7**, 18471

Received 29th August 2015,
Accepted 15th October 2015

DOI: 10.1039/c5nr05912g

www.rsc.org/nanoscale

Conductive polymer-mediated 2D and 3D arrays of Mn_3O_4 nanoblocks and mesoporous conductive polymers as their replicas†

Yoshitaka Nakagawa, Hiroyuki Kageyama, Riho Matsumoto, Yuya Oaki and Hiroaki Imai*

Orientation-controlled 2D and 3D microarrays of Mn_3O_4 nanocuboids that were mediated by a conductive polymer were fabricated by evaporation-induced self-assembly of the oxide nanoblocks and subsequent polymerization of pyrrole in the interparticle spaces. Free-standing mesoporous polypyrroles (PPy) having chain- and square-grid-like nanovoid arrays were obtained as replicas of the composite assemblies by dissolving the oxide nanoblocks. The PPy-mediated manganese oxide arrays exhibited stable electrochemical performance as an ultrathin anode of a lithium-ion secondary battery.

Introduction

A wide variety of nanoscale crystals, such as nanospheres, nanorods, and nanosheets, have been produced as building blocks of hierarchical architectures.[1–4] The well-ordered arrangements of monodisperse nanocrystals were formed from dispersion through an evaporation-induced assembly process.[5–7] Notably, cube-shaped nanocrystals that are covered with amphiphilic molecules tend to assemble in the same crystallographic direction as a single crystal.[8–13] Recently, 1D, 2D, and 3D microarrays have been achieved by controlling the direction and dimension of the self-assembly of rectangular nanoblocks.[14,15] The well-aligned ensembles of inorganic nanocrystals often exhibit interesting collective properties that are different from those displayed by individual nanocrystals and bulky large crystals.[16,17] Moreover, a combination of inorganic microarrays and organic polymers could provide fascinating functions. However, fabrication of the composite structures has not been reported. In the current study, we achieved 2D and 3D arrays of metal oxide nanoblocks mediated by a conductive polymer (Scheme 1).

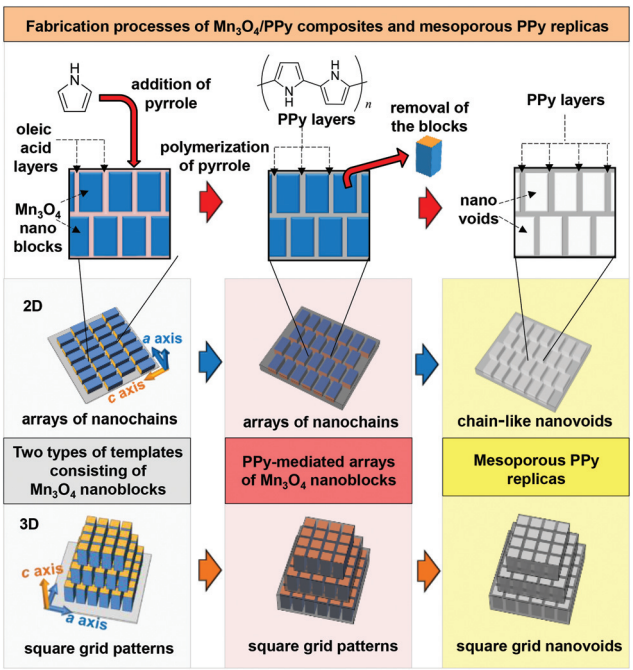

Scheme 1 Fabrication processes of ordered arrays of PPy-mediated Mn_3O_4 nanoblocks and their mesoporous PPy replicas having closed nanovoids.

The self-assembled nanospheres have been used as templates to produce elaborate porous replicas. Several replicas with hierarchical architectures and periodic macropores were fabricated by the introduction of polymers, oxides, or metals into the interparticle spaces and subsequent removal of the templates.[18–23] However, the size of the ordered voids prepared in the previous studies was larger than several hundreds of nanometers.[18–23] The highly ordered arrays consisting of rectangular nanoblocks are expected to be deformable templates for the fabrication of aligned voids several tens of nanometers in size. Here, we prepared nanovoid arrays of a conductive polymer using the well-ordered arrays of metal oxide nano-

Department of Applied Chemistry, Faculty of Science and Technology, Keio University, 3-14-1 Hiyoshi, Kohoku-ku, Yokohama 223-8522, Japan. E-mail: hiroaki@applc.keio.ac.jp

†Electronic supplementary information (ESI) available. See DOI: 10.1039/c5nr05912g

blocks. The mesoporous replicas were produced through dissolution of the nanoblocks from the ordered arrays combined with the polymer (Scheme 1).

In the current work, we focused on fabrication of the composite arrays consisting of polypyrrole (PPy)-mediated Mn_3O_4 nanocuboids. Manganese oxides have attracted much attention from a number of researchers as excellent electrode materials for manganese batteries, supercapacitors, and lithium-ion secondary batteries.[24–27] However, their low electrical conductivity and poor durability have interfered with their use as electrodes. Nanostructured electrodes have been widely expected to solve the problems described above because the nanoscale units can achieve short pathway distances for the transport of electrons and lithium ions.[28–31] Coating a conductive layer of carbon and polymers on the oxide surface was utilized to increase the electrical conductivity.[32–38] Here, the control of the self-assembly process of Mn_3O_4 rectangular nanoblocks has been applied to the design of appropriate nanostructures for electrode active materials. Moreover, the Mn_3O_4 nanocrystals arranged on a substrate were coated with PPy on a nanometric scale through polymerization of pyrrole at the air–solid interphase.[36] The electrochemical characteristics of ultrathin electrodes consisting of the PPy-mediated arrays of the nanoblocks were evaluated as lithium-ion battery anodes.

Experimental section

Synthesis of Mn_3O_4 rectangular nanoblocks

We prepared truncated Mn_3O_4 nanocuboids through a liquid–liquid two-phase (water and toluene) solvothermal method.[15] 0.60 mmol manganese(II) chloride and 35 wt% hydrogen peroxide (4 cm^3) were dissolved in 31 cm^3 of water in a 100 cm^3 Teflon container. Oleic acid (3.97 mmol) and *tert*-butylamine (2.31 mmol) were added into 30 cm^3 toluene. The organic mixture was added to the Teflon container without stirring. At this time, oxygen gas was generated through decomposition of hydrogen peroxide. When the generation of oxygen gas roughly stopped, the Teflon container was put into a stainless steel autoclave. The autoclave was heated at 115 °C for 12 h. After the reaction, the resultant dark brown liquid on the aqueous phase was transferred into a glass vial. A copper grid covered with a collodion film was placed on a piece of filter paper. A drop of the resultant dispersion was placed on the grid. After the excess medium of the dispersion was absorbed by the filter paper, the nanoblocks were deposited on the grid. Morphologies of nanocrystals were characterized by the transmission electron microscopy (TEM), high-resolution TEM (HRTEM), and fast Fourier transform (FFT) profiles using an FEI Tecnai-F20. The resultant dispersion and an equal amount of ethanol were mixed and then centrifuged at 13 500 rpm for 5 min. The precipitates were used for the powder X-ray diffraction (XRD) measurement (Rigaku MiniFlex II).

Fabrication and characterization of ordered arrays consisting of Mn_3O_4 rectangular nanoblocks

The resultant dispersion of Mn_3O_4 nanoblocks was centrifuged at 13 500 rpm for 5 min. The precipitates were redispersed into a hexane–toluene mixture (1 : 1 in volume) or toluene in a 6 cm^3 vial by ultrasonication for 30 min. The volume of the dispersions was 0.5 cm^3. The particle concentration was adjusted to 2.8×10^{-1} g dm^{-3} (2D arrays) or 5.6×10^{-1} g dm^{-3} (3D arrays). A silicon substrate (7 mm × 16 mm) treated with acetone by ultrasonication for 30 min was put in the dispersion in the vial. The dispersion spreads on the substrate by its surface tension. The dispersion medium was evaporated at room temperature. When the drying was completed, the morphologies of the products were observed *via* scanning electron microscopy (SEM) using an FEI-Sirion.

Fabrication and characterization of PPy-mediated arrays of Mn_3O_4 nanoblocks and their porous PPy replicas

The powder of 240 mg iron(III) nitrate nonahydrate ($Fe(NO_3)_3 \cdot 9H_2O$), the neat liquid of 1 cm^3 pyrrole (C_4H_5N), and the ordered arrays of Mn_3O_4 nanoblocks deposited on the substrate were separately placed in a glass bottle. The glass bottle was covered with a container slightly larger than the bottle to prevent leaking of pyrrole vapor. After sealing the sample bottle and container, the container was heated at 60 °C for 3 h. After the reaction, the color of the walls of the sample bottle and the substrate changed to black. PPy-mediated arrays of Mn_3O_4 nanoblocks formed on the substrate were peeled off by immersing the black substrate in 0.5 cm^3 ethanol by ultrasonication for 10 min. Porous PPy films were fabricated by immersing the black substrate in 0.5 cm^3 hydrochloric acid (dilute HCl, 2 mol dm^{-3}) by ultrasonication for 1 h. A copper grid was immersed in the dispersion of PPy films. After removing the grid from the dispersion, the excess liquid adhering to the grid was absorbed by a filter paper. The morphologies and composition of the products deposited on the grid were characterized by TEM and Energy-dispersive X-ray (EDX) analyses. Fourier transform infrared (FTIR) spectra were obtained by using a Jasco FT/IR-4200. Commercial PPy powder (Aldrich) was used as a reference.

Electrochemical characterization of ordered arrays of Mn_3O_4 nanoblocks and PPy-mediated arrays of Mn_3O_4 nanoblocks

The electrochemical performance was measured with a beaker-type three-electrode cell. The working electrode was ordered arrays of Mn_3O_4 nanoblocks or PPy-mediated arrays of Mn_3O_4 fabricated on a copper substrate. A lithium metal was used for the counter and reference electrodes on a copper mesh. 1 mol dm^{-3} of $LiClO_4$ in ethylene carbonate and diethyl carbonate (1/1 volume) was used as the electrolyte. The cell was assembled in an argon-filled glove box. Discharge–charge measurements were performed in a potential range between 0.1 and 3.0 V *vs.* Li/Li^+ at room temperature. The current density for the charge and discharge reactions was increased from 0.25 C to 10 C (1 C = 117 mA g^{-1}).

Results and discussion

Truncated nanocuboids obtained by the two-phase solvothermal method were assigned to tetragonal Mn_3O_4 by XRD analysis and HRTEM images as reported in our previous work (Fig. S1†).[15] The resultant anisotropic nanoblocks were covered with oleic acid molecules. The typical width and length of the Mn_3O_4 nanocuboids synthesized under the standard conditions were ~10 nm and ~20 nm, respectively. 2D ordered arrays of the Mn_3O_4 rectangular nanoblocks were fabricated on a silicon substrate from a dispersion of the cuboids by evaporation of a mixed medium of toluene and hexane (1 : 1 in volume). The 2D ordered structures with their *a* faces parallel to the substrate were observed by SEM (Fig. 1a and b). Adsorbed molecular layers ~3 nm thick existed between adjacent nanoblocks in the ordered arrays as we reported in our previous article.[15]

By the introduction of PPy into the interparticle spaces through polymerization of the vaporized pyrrole, the polymer-mediated 2D arrays were achieved. As reported in our previous work, amorphous PPy was formed around nanocrystals by the polymerization method (Fig. S2†).[36] We characterized the resultant films by TEM and EDX analyses. The ordered 2D arrays (Fig. 1c and d) similar to the original structures (Fig. 1a and b) were observed after the polymerization. Manganese from the oxide cuboids and nitrogen originating from PPy were detected in the composite films (Fig. 1g, upper spectrum).

Fig. 1h shows FTIR spectra of the Mn_3O_4 nanoblock arrays before and after PPy coating. Specific absorption peaks due to PPy in FTIR spectra indicate the presence of the polymer in the composite samples.[39] Thus, the 2D ordered arrays of Mn_3O_4 nanocuboids were mediated by PPy. Moreover, the absorption bands in 1500–1800 and 2800–3000 cm^{-1} indicate the existence of oleic acid in the nanoblock arrays even after the PPy coating. As shown in Fig. 1h, FTIR signals assigned to PPy in the composites are observed to be highly broadened by hybridization. This indicates that the framework of PPy strongly interacts with alkyl chains of oleic acid covering the nanoblock surface. The Py monomers penetrated into the interparticular layer and then polymerized among the nanoblocks.

After the Mn_3O_4/PPy composite films were immersed in a dilute HCl solution, the 2D arrays remained in the films as shown in TEM images (Fig. 1e and f). However, manganese was not detected in the films by EDX analysis (Fig. 1g, lower spectrum). Therefore, the porous structures of PPy consisting of chain-like nanoscale voids were formed through dissolution of the Mn_3O_4 nanoblocks from the composites.

After the dissolution of Mn_3O_4 nanoblocks, we detected chlorine and oxygen that originated from residual HCl and oleic acid in the PPy films, respectively.

Self-standing films of Mn_3O_4 nanoblocks/PPy composites and porous PPy replicas were obtained by removal of the support substrates (Fig. 2a and b). The crystalline phase of nanoblocks remained unaltered after the polymerization of

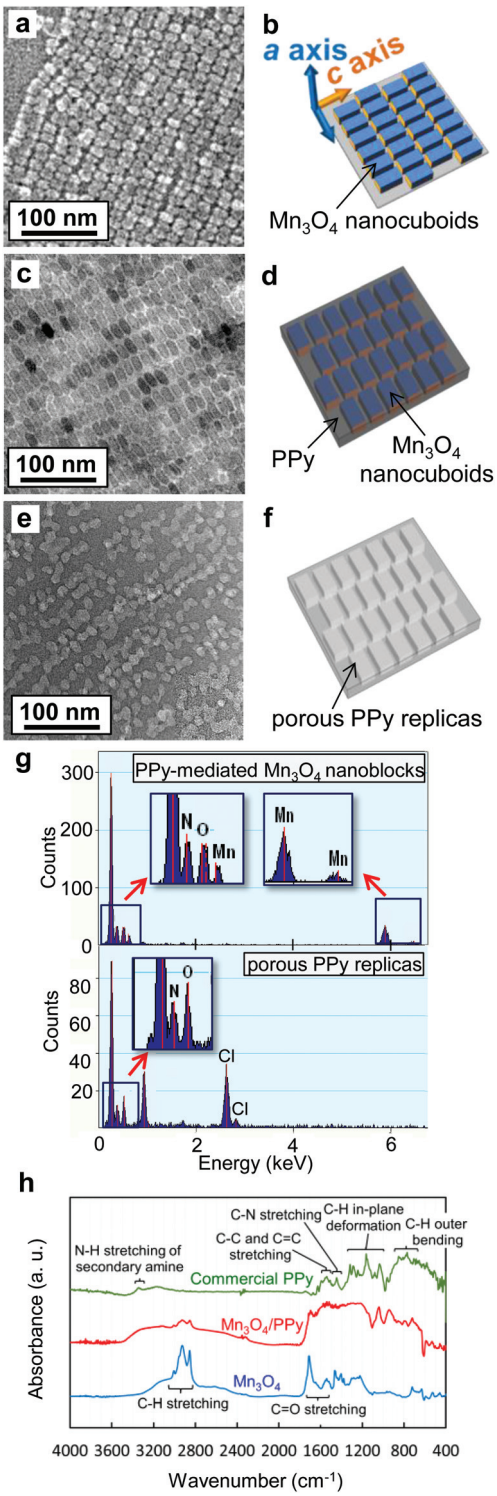

Fig. 1 SEM image and schematic illustration of 2D arrays with *a* faces of Mn_3O_4 nanoblocks parallel to a substrate (a, b). TEM image and schematic illustration of PPy-mediated arrays of Mn_3O_4 nanoblocks (c, d). TEM image and schematic illustration of a PPy replica (e, f). EDX spectra (g) and FTIR spectra (h) of the PPy-mediated arrays of Mn_3O_4 nanoblocks and the PPy replica.

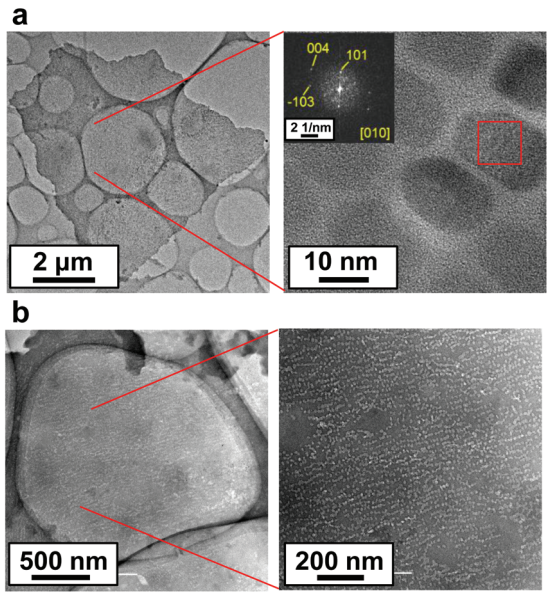

Fig. 2 TEM and HRTEM images of self-standing PPy-mediated arrays of Mn_3O_4 nanoblocks and FFT pattern corresponding to the lattice fringes of a Mn_3O_4 nanoblock (red square region) (a). TEM images of a PPy replica film (b).

pyrrole because the fast Fourier transform (FFT) patterns corresponding to the lattice fringes of the nanoblocks in the composite film were assigned to tetragonal Mn_3O_4 (inset of Fig. 2a).

When toluene was used as a dispersion medium, 3D arrays with their *c* faces of Mn_3O_4 parallel to the substrate were obtained (Fig. 3a and b).[15]

We obtained square grid patterns consisting of Mn_3O_4 nanocuboids. The ordered PPy-mediated 3D arrays of Mn_3O_4 nanoblocks with the same square grid patterns were produced through the introduction of the polymer into interparticle spaces (Fig. 3c, d and g). The 3D PPy replicas having square-grid-like nanovoid arrays were produced by subsequent dissolution of the Mn_3O_4 nanocuboids (Fig. 3e, f, and g).

The charge–discharge reactions with lithium ions were performed using the PPy-mediated 2D and 3D arrays of Mn_3O_4 nanoblocks fabricated on a copper substrate. The typical discharge curves of Mn_3O_4 were observed with the plateaus at 0.5 V (Fig. 4a). The PPy-mediated 2D arrays of Mn_3O_4 nanoblocks showed improved specific capacity and stable cycling performance as compared to uncoated 2D arrays of Mn_3O_4 nanoblocks (Fig. 4b).

The first and second discharge capacities of the ultrathin film electrode of 5- or 6-layered nanoblocks (3D arrays ~100 nm in thickness)/PPy composites were ~1170 mA h g^{-1} at a current density of 0.25 C. At a high current density (10 C), discharge and charge capacities were over 400 mA h g^{-1}. When the current density was returned back to 0.25 C, the ultrathin film electrode exhibited stable reversible capacities of around 900 mA h g^{-1}, which is close to the theoretical capacity for the fully reversible conversion reaction. The electrochemical

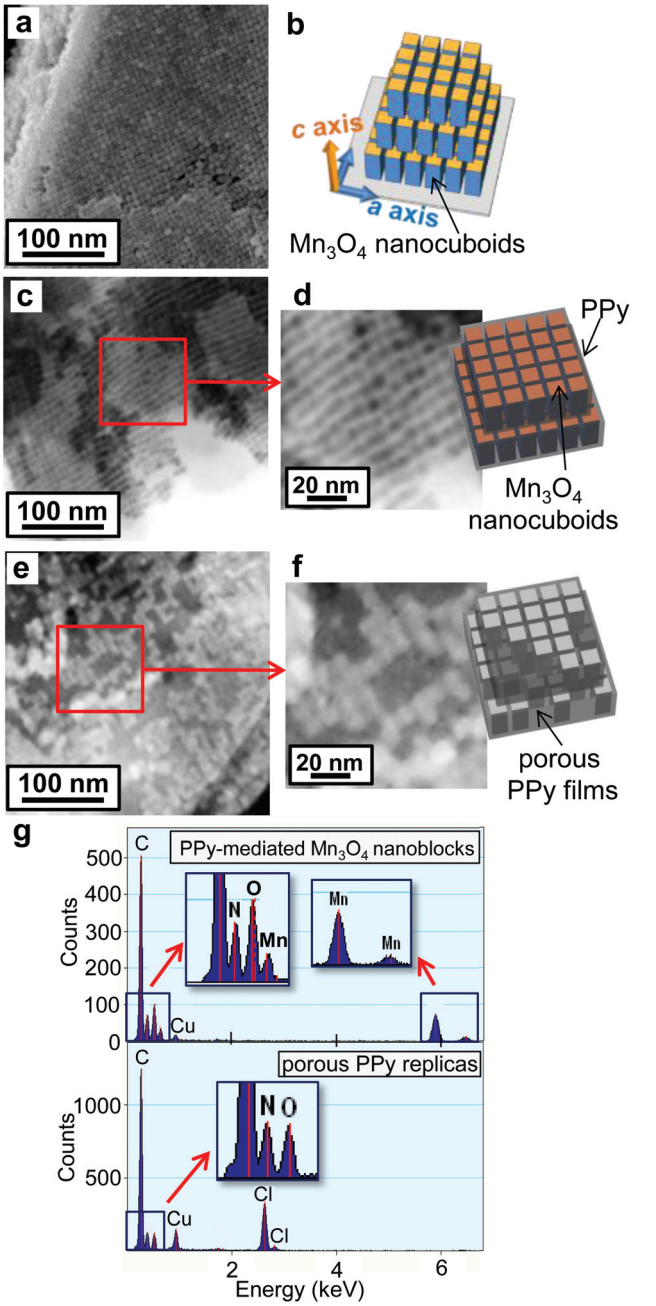

Fig. 3 SEM image and schematic illustration of 3D arrays with *c* faces of Mn_3O_4 nanoblocks parallel to a substrate (a, b). Black/white inverted STEM images and schematic illustration of PPy-mediated arrays of Mn_3O_4 nanoblocks (c, d). Black/white inverted STEM images and schematic illustration of a PPy replica (e, f). EDX spectra of PPy-mediated arrays of Mn_3O_4 nanoblocks and the PPy replica (g).

capacities of the PPy-mediated 3D arrays of Mn_3O_4 nanoblocks are almost the same as that of Mn_3O_4 particles in the conventional system.[26,30] The improvement is ascribed to the enhanced electron conductivity and stabilization of the nanocrystals on the conductive substrate in the presence of PPy that mediates Mn_3O_4 nanoblocks.

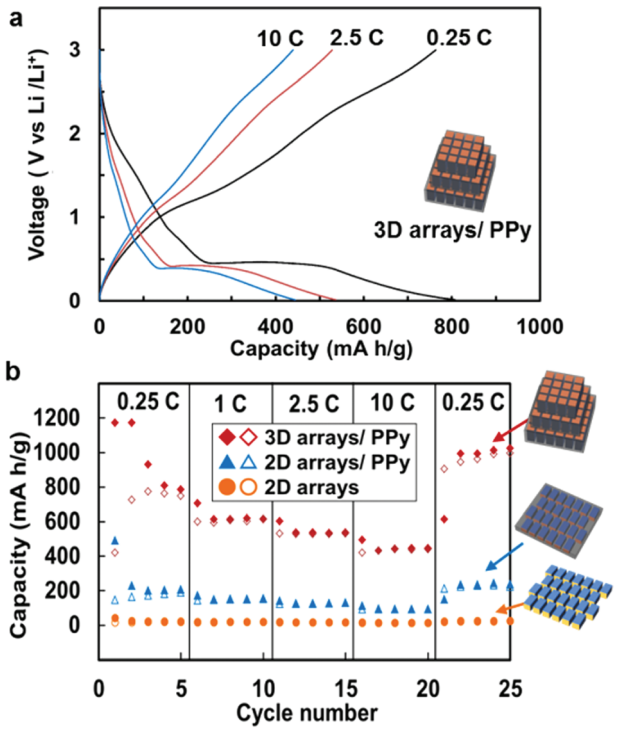

Fig. 4 Charge and discharge curves of PPy-mediated 3D arrays of Mn_3O_4 nanoblocks fabricated on a copper substrate at the current density of 0.25 C at 4th cycle, 2.5 C at 14th cycle, and 10 C at 19th cycle (1 C = 117 mA g^{-1}) (a). Charge and discharge capacities of 2D ordered arrays of Mn_3O_4 nanoblocks (circles), PPy-mediated 2D arrays of Mn_3O_4 nanoblocks (triangles), and PPy-mediated 3D arrays of Mn_3O_4 nanoblocks (squares) according to the cycle number (b). (Charge and discharge capacities are represented by non-filled and filled geometric symbols, respectively).

Conclusions

In this study, we fabricated 2D and 3D ordered arrays of Mn_3O_4 nanocuboids that were mediated by the conductive polymer by the polymerization of pyrrole in interparticle spaces. Self-standing mesoporous PPy replicas having chain- and square-grid-like nanovoid arrays were obtained from different types of PPy-mediated Mn_3O_4 nanoblocks. The dimension- and direction-controlled assembly of anisotropic nanoblocks is useful for the deformable template to regulate nanoscale morphologies of a wide variety of polymers. The ultrathin anodes of PPy-mediated 3D Mn_3O_4 nanoblock arrays exhibited stable electrochemical performance and excellent discharge–charge capacities for a lithium-ion battery.

Acknowledgements

This work was partially supported by the Advanced Low Carbon Technology Research and Development Program (ALCA) from Japan Science and Technology Agency (JST), a Grant-in-Aid for Challenging Exploratory Research (Grant 15K14129), and a Grant-in-Aid for Scientific Research (Grant 22107010) on Innovative Areas of "Fusion Materials: Creative Development of Materials and Exploration of Their Function through Molecular Control" (Area no. 2206) from the Ministry of Education, Culture, Sports, Science and Technology.

References

1 S. A. Harfenist, Z. L. Wang, M. M. Alvarez, I. Vezmar and R. L. Whetten, *J. Phys. Chem.*, 1996, **100**, 13904.
2 K. An, N. Lee, J. Park, S. C. Kim, Y. Hwang, J.-G. Park, J.-Y. Kim, J.-H. Park, M. J. Han, J. Yu and T. Hyeon, *J. Am. Chem. Soc.*, 2006, **128**, 9753.
3 T. Wang, J. Zhuang, J. Lynch, O. Chen, Z. Wang, X. Wang, D. LaMontagne, H. Wu, Z. Wang and Y. C. Cao, *Science*, 2012, **338**, 358.
4 Y. C. Cao, *J. Am. Chem. Soc.*, 2004, **126**, 7456.
5 T. P. Bigioni, X.-M. Lin, T. T. Nguyen, E. I. Corwin, T. A. Witten and H. M. Jaeger, *Nat. Mater.*, 2006, **5**, 265.
6 M. Li, Y. Chen, N. Ji, D. Zeng and D.-L. Peng, *Mater. Chem. Phys.*, 2014, **147**, 604.
7 T. Ming, X. Kou, H. Chen, T. Wang, H.-L. Tam, K.-W. Cheah, J.-Y. Chen and J. Wang, *Angew. Chem.*, 2008, **120**, 9831, (*Angew. Chem., Int. Ed.*, 2008, **47**, 9685).
8 A. Demortière, P. Launois, N. Goubet, P.-A. Albouy and C. Petit, *J. Phys. Chem. B*, 2008, **112**, 14583.
9 J. Zhang, H. Yang, K. Yang, J. Fang, S. Zou, Z. Luo, H. Wang, I.-T. Bae and D. Y. Jung, *Adv. Funct. Mater.*, 2010, **20**, 3727.
10 T. Wang, X. Wang, D. LaMontagne, Z. Wang, Z. Wang and Y. C. Cao, *J. Am. Chem. Soc.*, 2012, **134**, 18225.
11 C.-J. Chen, R.-K. Chiang and Y.-R. Jeng, *J. Phys. Chem. C*, 2011, **115**, 18142.
12 C.-W. Liao, Y.-S. Lin, K. Chanda, Y.-F. Song and M. H. Huang, *J. Am. Chem. Soc.*, 2013, **135**, 2684.
13 M. Agthe, E. Wetterskog, J. Mouzon, G. Salazar-Alvarez and L. Bergström, *CrystEngComm*, 2014, **16**, 1443.
14 M. Rycenga, J. M. McLellan and Y. Xia, *Adv. Mater.*, 2008, **20**, 2416.
15 Y. Nakagawa, H. Kageyama, Y. Oaki and H. Imai, *J. Am. Chem. Soc.*, 2014, **136**, 3716.
16 S. Sun, C. B. Murray, D. Weller, L. Folks and A. Moser, *Science*, 2000, **287**, 1989.
17 A. Martin, C. Schopf, A. Pescaglini, J. J. Wang and D. Iacopino, *Langmuir*, 2014, **30**, 10206.
18 L.-Y. Yang and W.-B. Liau, *Macromol. Chem. Phys.*, 2007, **208**, 994.
19 K. Yoshino, S. B. Lee, S. Tatsuhara, Y. Kawagishi, M. Ozaki and A. A. Zakhidov, *Appl. Phys. Lett.*, 1998, **73**, 3506.
20 F. Li, Z. Wang, N. S. Ergang, C. A. Fyfe and A. Stein, *Langmuir*, 2007, **23**, 3996.
21 G. Guan, R. Zapf, G. Kolb, Y. Men, V. Hessel, H. Loewe, J. Ye and R. Zentel, *Chem. Commun.*, 2007, 260.
22 N. R. Denny, S. E. Han, D. J. Norris and A. Stein, *Chem. Mater.*, 2007, **19**, 4563.

23 S.-J. Huang and P.-Y. Chen, *Electrochim. Acta*, 2013, **89**, 180.
24 K. Kordesh and M. Weissenbacher, *J. Power Sources*, 1994, **51**, 61.
25 B. Ammundsen and J. Paulsen, *Adv. Mater.*, 2001, **13**, 943.
26 X. Fang, X. Lu, X. Guo, Y. Mao, Y.-S. Hu, J. Wang, Z. Wang, F. Wu, H. Liu and L. Chen, *Electrochem. Commun.*, 2010, **12**, 1520.
27 J. Bhagwan, A. Sahoo, K. Lal Yadav and Y. Sharma, *Electrochim. Acta*, 2015, **174**, 992.
28 A. S. Aricò, P. G. Bruce, B. Scrosati, J.-M. Tarascon and W. Van Schalkwijk, *Nat. Mater.*, 2005, **4**, 366.
29 J. Wang, N. Du, H. Wu, H. Zhang, J. Yu and D. Yang, *J. Power Sources*, 2013, **222**, 32.
30 J. Gao, M. A. Lowe and H. D. Abruna, *Chem. Mater.*, 2011, **23**, 3223.
31 H. Kageyama, Y. Oaki and H. Imai, *RSC Adv.*, 2014, **4**, 44124.
32 Y. Piao, H. S. Kim, Y.-E. Sung and T. Hyeon, *Chem. Commun.*, 2010, **46**, 118.
33 Z. Yang, J. Shen, N. Jayaprakash and L. A. Archer, *Energy Environ. Sci.*, 2012, **5**, 7025.
34 C. Wang, L. Yin, D. Xiang and Y. Qi, *ACS Appl. Mater. Interfaces*, 2012, **4**, 1636.
35 B. Jang, M. Park, O. B. Chae, S. Park, Y. Kim, S. M. Oh, Y. Piao and T. Hyeon, *J. Am. Chem. Soc.*, 2012, **134**, 15010.
36 R. Muramatsu, Y. Oaki, K. Kuwabara, K. Hayashi and H. Imai, *Chem. Commun.*, 2014, **50**, 11840.
37 Z. Cai, L. Xu, M. Yan, C. Han, L. He, K. Mulonda Hercule, C. Niu, Z. Yuan, W. Xu, L. Qu, K. Zhao and L. Mai, *Nano Lett.*, 2015, **15**, 738.
38 L. Zhang, K. Zhao, W. Xu, Y. Dong, R. Xia, F. Liu, L. He, Q. Wei, M. Yana and L. Mai, *Phys. Chem. Chem. Phys.*, 2015, **17**, 7619.
39 K. Majid, R. Tabassum, A. F. Shah, S. Ahmad and M. L. Singla, *J. Mater. Sci. Mater. Electron.*, 2009, **20**, 958.